# Raman Amplification with a Flying Focus

Introduction

Continuing to push the boundary of laser intensity using existing technology is increasingly challenged by the need for large, efficient, and damage-resistant gratings. Here, we propose a new laser amplifier scheme utilizing stimulated Raman scattering in plasma in conjunction with a "flying focus"—a chromatic focusing system combined with a chirped pump beam that provides spatiotemporal control over the pump's focal spot.[1] Localized high intensity is made to propagate at $v = -c$ just ahead of the injected counter-propagating seed pulse. By setting the intensity in the interaction region to be just above the ionization threshold, an ionization wave is produced that travels at a fixed distance ahead of the seed. Simulations show that this will make it possible to optimize the plasma temperature and mitigate many of the issues that are known to have impacted previous Raman amplification experiments, in particular the growth of precursors.

Plasma-based laser amplifiers utilizing either stimulated Raman scattering[2] (SRS) or strongly coupled stimulated Brillouin scattering[3–8] have long been of interest. Lacking a damage threshold, compact plasma-based systems could produce unfocused intensities $I \approx 10^{17}$ W/cm^2—more than six orders of magnitude larger than conventional systems. Typically, a moderate-intensity pump pulse with a duration of at least $2L/c$ propagates across a plasma of length L. When the pump's leading edge reaches the end of the plasma, an initially weak seed pulse is injected in a counter-propagating geometry. Tuned to satisfy the Manley–Rowe frequency- and wave-number–matching conditions, the beat wave between the two beams drives a plasma wave that mediates energy transfer from the pump to the seed (c.f., Fig. 151.8). While early work[9–12] on Raman-based plasma amplifiers appeared promising, progress has slowed and numerous attempts have been made recently to elucidate the shortcomings of experiments. A consensus is emerging that thermal effects[13–20] and the amplification of precursors growing from noise ahead of the seed pulse[13,21–25]—issues that are both related to the pump's traversal of ionized plasma prior to meeting the seed—may be among the most pervasive issues that degrade performance.
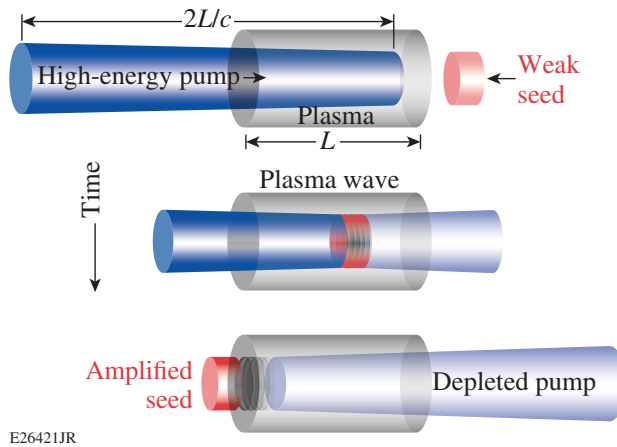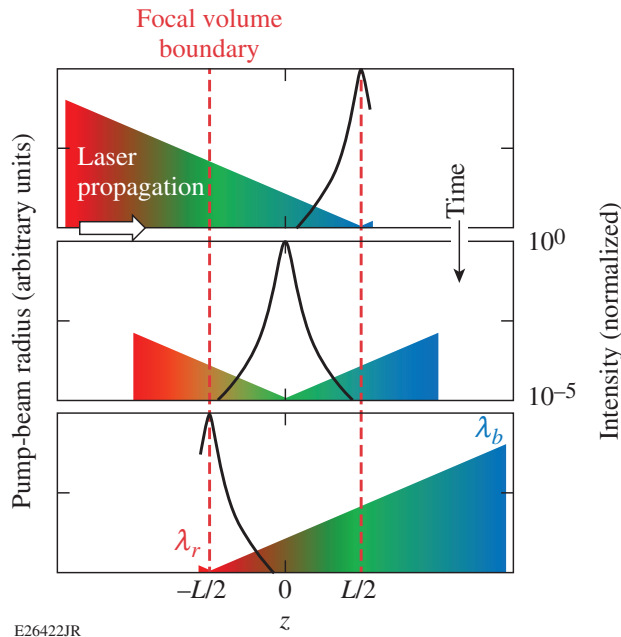

Figure 151.8
A moderate-intensity pump pulse with a duration of at least $2L/c$ propagates across a plasma of length L. When the pump's leading edge reaches the end of the plasma, an initially weak seed pulse is injected in a counter-propagating geometry. Tuned to satisfy the Manley–Rowe frequency- and wave-number–matching conditions, the beat wave between the two beams drives a plasma wave that mediates energy transfer from the pump to the seed.

An alternate scheme has been proposed to mitigate precursor growth in which the seed ionizes the plasma coincident with its amplification by the pump.[26] However, this introduces additional constraints: the pump intensity must be below the threshold for ionization, limiting the Raman growth rate; conversely, the initial seed intensity must be high enough to photoionize the plasma, limiting the degree to which it can be further amplified; and the ionization itself damps the growing seed pulse. To our knowledge, this scheme has yet to be tested because of the added complexity.

A Raman amplifier with a flying focus retains the advantages of seed ionization while eliminating its downsides. A chirped pump is focused by a diffractive lens that introduces chromatic aberration in order to produce a longitudinally distributed focal spot. The temporal dispersion provided by the chirp, combined with the spatial dispersion provided by the lens, provides spatiotemporal control over the propagation of intensity isosurfaces. In the example shown in Fig. 151.9,

Figure 151.9
A negatively linearly chirped pump combined with a chromatic focusing system causes the high-intensity focus to propagate backward at $v \approx -c$ when the pump duration is $2L/c$, where L is the distance between the foci of the pump's bandwidth extrema.

the pump has a negative linear chirp and a pulse duration that is equal to $T = 2L/c$, where L is both the length of the focal region spanned by its bandwidth and the length of the amplifier interaction region. In this case, the desired pump intensity first appears where the pump exits the interaction region and subsequently propagates backward at $v \approx -c$ at a constant value over a length that can be many times the Rayleigh length. More details regarding the flying focus optical system, along with additional applications, are contained in the companion article **Flying Focus: Spatiotemporal Control of the Laser Focus**, p. 115.[1]

To demonstrate the benefits of this concept, the coupled three-wave equations describing SRS in plasma were solved numerically (see, e.g., Refs. 13 and 26 and references therein). Such models have previously been benchmarked against particle-in-cell simulations and found to be in good agreement when plasma-wave amplitudes were kept below the wave-breaking limit and kinetic effects could be ignored [at low $k_3\lambda_{De} \le 0.3$, where k_3 is the electron plasma wave's (EPW's) wave number and λ_{De} is the Debye length].[27] The three-wave model is supplemented with a field ionization model to simulate the plasma ionization by the pump.[26] The model is described in much greater detail in **Methods**, p. 125.

For all of the simulations, the initial density of hydrogen atoms was 6×10^{18} cm^{-3} and the interaction length was 4 mm, defining a pump duration of 26.7 ps. The pump wavelength was $\lambda = 1$ μm and the seed was upshifted by the EPW frequency. For the flying focus Raman amplification (FFRA) base case, the pump focusing system was $f/5$ with the focus of each color located past the interaction region. To simulate focusing in this 1-D model, the pump enters from the left edge and its intensity increases as it propagates to the right in a manner that is consistent with the f number of the system. The blue leading edge of the pump converges to a spot diameter of 400 μm at the exit of the interaction region, where the intensity was set to be $I_1 = 1.4 \times 10^{14}$ W/cm^2.

In the simulations, the plasma mediating the energy transfer was formed by the pump beam ionizing the hydrogen gas within the interaction region. The ionization threshold of hydrogen is very close to the optimal pump intensity in systems designed for $\lambda \approx 1$-μm lasers. Since the pump first reaches this intensity at the right edge of the amplifier in the case of FFRA, plasma is initialized there and an ionization wave subsequently propagates backward with the intensity isosurface. The setup can therefore be tuned so that the plasma is formed just before the seed arrival at every point along the interaction region.

The peak of a 500-fs-duration (full width at half maximum) seed pulse with an initial intensity $I = 1 \times 10^{11}$ W/cm^2 was injected at the right edge just after the arrival of the pump's leading edge ($t = 14$ ps). Figure 151.10(a) shows three snapshots of the interaction as the injected seed travels from right to left across the interaction region for the FFRA case. The first frame shows that the gas is ionized only $(n_e/n_c > 0)$ close to the right edge, where the pump first reaches high intensity. The seed duration stretches as it grows in the linear regime. From the first to the second frame, it is clear that the ionization wave is propagating at an approximately fixed distance ahead of the seed. The nonlinear pump-depletion regime has been reached, with seed pulse compression and the formation of a secondary peak. This efficient amplification continues in the final frame. These results demonstrate the ideal behavior that is expected when the seed enters unperturbed plasma and competing instabilities are avoided.

Contrast Fig. 151.10(a) with the behavior observed in Fig. 151.10(b), which shows the results from a Raman amplifier without the flying focus. In this case, the intensity was set to $I = 1.4 \times 10^{14}$ W/cm^2 at the left edge of the amplifier and was assumed to be collimated as it propagated from left to right (consequently, the pump intensity seen by the seed pulse
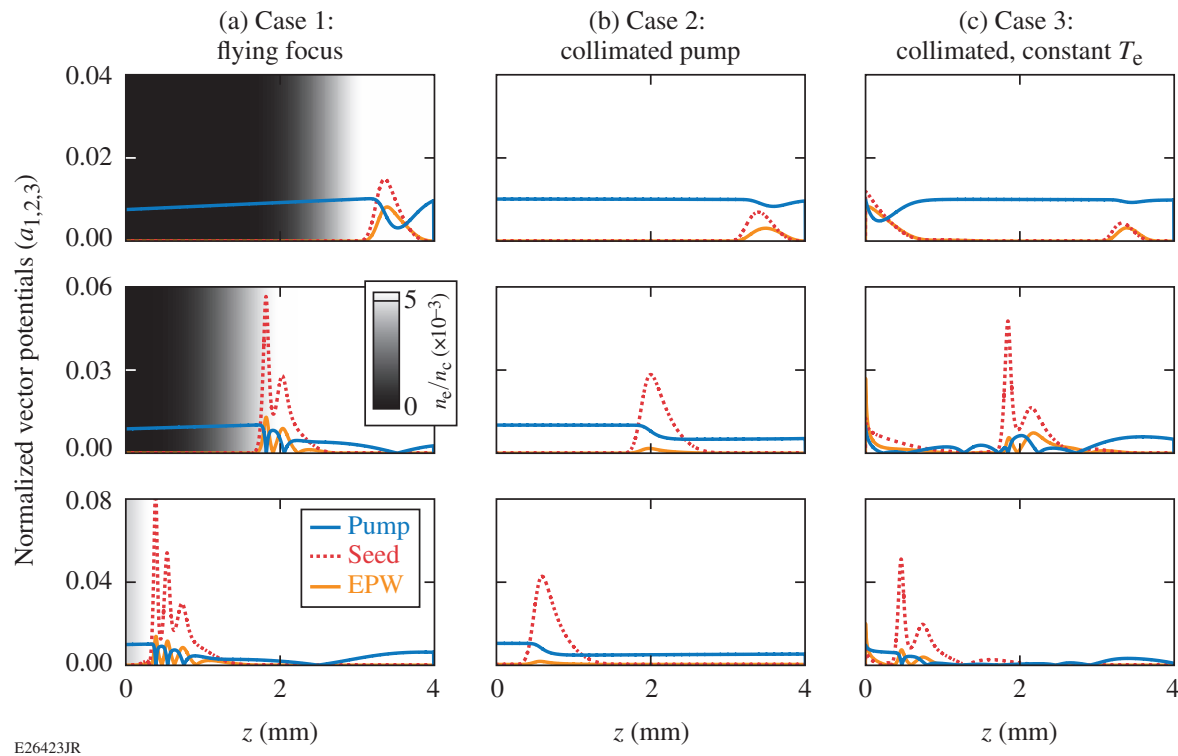
Figure 151.10
Results of three-wave model simulations. (a) With the flying focus, the pump first reaches high intensity at the right edge, where ionization is initialized. Constant intensity moves at $v = -c$ as different colors converge to different locations, so the ionization wave propagates at a nearly fixed distance ahead of the injected seed pulse. Ideal plasma amplifier behavior is observed. (b) When the pump is collimated within the interaction region and above threshold for ionization, the seed encounters higher temperatures along nearly its entire path, which reduces growth via increased Landau damping. (c) With a collimated beam as in Case 2 but holding T_e fixed to be similar to Case 1, spontaneous stimulated Raman scattering (SRS) grows during the long time in which the pump propagates across the ionized plasma. Premature pump depletion degrades the resulting seed amplification. Flying focus Raman amplification (FFRA) Case 1 with noise initialized at the same level did not produce such precursors. EPW: electron plasma wave.

is nearly the same in both cases). The first frame shows that upon reaching the right edge, the plasma is ionized everywhere throughout the interaction region. While growth in the first frame is comparable, it slows rapidly compared to FFRA. Pump depletion and pulse compression fail to occur in this case.

The difference can be understood by looking at the electron temperature encountered by the peak of the seed pulse versus time [Fig. 151.11(a)]. In FFRA "Case 1," after a brief initial growth period, T_e levels off at ≈ 45 eV because of the nearly constant duration of plasma heating by the pump prior to the seed's arrival at each point along its path. With standard focusing (or a preformed plasma), the seed encountered plasma that was heated for a progressively longer duration as it propagated, producing a strong gradient in T_e (Case 2). This model captures the fact that excessive heating can lead to debilitating levels of collisionless Landau damping, which acts to suppress the seed growth.[13,15] Figure 151.11(b) shows the sum of collisional and collisionless damping as a function of temperature. The former

dominates at low temperatures and the latter at high temperatures; FFRA Case 1 is close to the temperature at which EPW damping is minimized.

Note that there could be additional impacts of elevated temperature that are not captured by this model. The thermal gradient seen by the seed pulse can lead to resonance detuning resulting from the Bohm–Gross frequency shift.[14] Detuning can also result from the kinetic nonlinear frequency shift that accompanies particle trapping.[16,19,25] Perhaps most importantly, the wave-breaking threshold is reduced in warm plasma,[17–19,28] which limits the plasma-wave amplitudes and thereby the energy transfer from pump to seed. This model, therefore, likely underestimates the adverse effects of high temperature and lack of temperature control with a conventional focusing and ionization scheme.

Given the uncertainties, a temperature of ≈ 45 eV may not be optimal. A nice feature of the FFRA scheme, however,
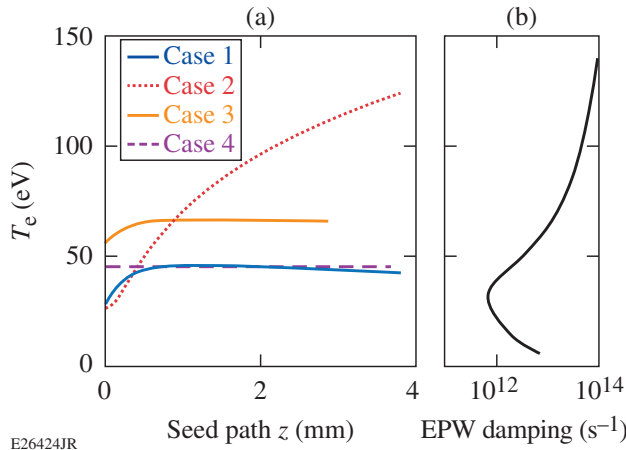
E26424JR

Figure 151.11

(a) In Case 1, the temperature encountered by the seed was nearly constant everywhere because of the ionization wave propagating ahead of the seed. In Case 2, the seed encountered progressively higher temperatures because each slice of plasma was heated for a longer duration. Case 3 used the flying focus (like Case 1) but delayed the seed injection by 3 ps, which shows that T_e is tunable. Case 4 used a collimated pump (like Case 2), but T_e was artificially fixed to be similar to Case 1; this case illustrates the negative effect of precursor growth. (b) The electron plasma wave damping is minimized around $T_e \approx$ 40 eV, so the FFRA scheme can be tuned to operate close to this temperature.

is that the temperature can be easily tuned by adjusting the delay between the ionization wave and the injected seed pulse. Many parameters can influence this delay. Holding all else constant but injecting the seed 3 ps later, its peak encounters an electron temperature that is uniformly higher by ~20 eV [c.f., Fig. 151.11(a), Case 3]. Because of the higher temperature, it takes longer to reach pump depletion and the secondary peaks are suppressed. Both the interaction pump intensity relative to the ionization threshold of the gas and the pump's f number are additional parameters for tuning the delay between ionization and seed injection.

To investigate nonthermal differences between FFRA and standard Raman amplifiers, a Case 4 was run, repeating Case 2 but with a fixed electron temperature ($T_e = 45$ eV). Although the seed encountered a similar electron temperature everywhere in Cases 1 and 4, the pump spent a longer time in ionized plasma prior to seed injection in Case 4 compared to FFRA Case 1. The debilitating effect of spontaneous SRS growing ahead of the seed is observed in Fig. 151.10(c). Although seed growth over the first half of the plasma proceeds in a similar fashion as Case 1, subsequent growth is suppressed because of premature pump depletion and interference with pre-existing EPW's. Although noise was included in the same manner in FFRA Case 1, no spontaneous SRS growth was observed because of the limited distance over which it could grow ahead of the seed.

As with temperature, this model likely underestimates the negative impacts of spontaneous SRS. While the zeroth-order effect is competition for pump energy,[13] there is some evidence that saturation of even low-level precursors can corrupt plasma conditions (e.g., with driven ion-acoustic waves or modified electron distribution functions) over relatively long time scales.[23,24] In these situations, the seed does not encounter quiescent plasma and its growth is compromised. The controlled introduction of frequency detuning has been proposed to mitigate precursors without precluding the desired seed amplification (resulting from the larger resonance bandwidth of the latter in the nonlinear pump-depletion regime).[21,22] Despite evidence that modern experiments have been adversely affected by too much frequency detuning,[18] spontaneous SRS continues to be an issue and was recently observed to dominate the overall backscatter as the Raman growth rate was increased.[25]

The use of a chirped pump beam—a feature of many previous experiments[10–12,15,23,24] is necessary for the flying focus but does introduce some frequency detuning for fixed plasma conditions that could degrade performance.[18] It could be compensated for, however, by introducing a density gradient along the seed path in order to exactly satisfy the frequency-matching condition everywhere. While perfect resonance may result in undue levels of spontaneous SRS in a typical plasma amplifier,[21,22] it would not degrade FFRA because of the alternative means by which FFRA suppresses precursor growth.

Methods

The basic three-wave equations are

$$(\partial_t - v_1\partial_x + \nu_1)a_1 = Ka_2a_3,$$

$$(\partial_t - v_2\partial_x + \nu_2)a_2 = Ka_2a_3^*, \qquad (1)$$

$$(\partial_t - v_3\partial_x + \nu_3 + i\delta\omega)a_3 = Ka_1a_2^* + S_3,$$

where the subscripts 1, 2, and 3 refer to the pump, the seed, and the EPW, respectively; v_i's are group velocities; ν_i's are damping rates; $K = \omega(n_e/n_c)^{1/4}/2$ is the wave-coupling parameter, where n_e is the electron density and n_c is the critical density; $a_{1,2} = 0.855 \times 10^3 \lambda_{1,2}(\mu m)\sqrt{I_{1,2}(W/cm^2)}$ are normalized laser vector potentials, and $a_3 = |e|\langle E_3\rangle/m_ec\sqrt{\omega\omega_{pe}}$ is the normalized envelope of the EPW, with pump frequency ω and EPW frequency ω_{pe}. Advection of the plasma wave can be neglected ($v_3 \approx 0$), and here detuning was also neglected ($\delta\omega = 0$) since it has been explored

extensively elsewhere.[13,14,18,21,22] The pump and seed are damped collisionally, $\nu_{1,2} = \nu_{ei}(\omega_{pe}^2/\omega^2)$ with $\nu_{ei} = 2.9 \times 10^{-6} Zn_e$ (cm^{-3}) ΛT_e (eV)$^{-3/2}$; $\nu_3 = \nu_{ei} + \nu_L$ includes both collisional absorption and collisionless (Landau) damping, with $\nu_L \approx \sqrt{\pi/2}\left[\omega_{pe}^4/(k_3 v_e)^3\right]\exp\left[-\omega_{pe}^2/2(k_3 v_e)^2\right]$. S_3 is a noise term that is included to investigate spontaneous SRS growing from undriven plasma fluctuations. Following Ref. 13, $S_3 = c_1 \nu_3 T_e$ is assumed to be proportional to the EPW damping rate and electron temperature, but a multiplier c_1 was added to test the sensitivity to the initial noise level. Experiments often find that plasma fluctuations are elevated over the expected thermal levels.

The three-wave model was supplemented with an ionization model to simulate the plasma ionization by the pump[26]

$$\partial_t n_e = n_n w(a_1),$$

$$\partial_t n_n = -n_n w(a_1),$$
(2)

where n_n is the neutral gas density and $w(a_1)$ is the ionization rate that depends on the local pump intensity. In the regime of interest, the Keldysh formula is valid.[29,30] For $\gamma = \sqrt{2U_I/m_e c^2}/a_1 \gg 1$, where U_I is the ionization potential, the multiphoton ionization rate $w(a) \cong \omega N^{3/2}(2\gamma)^{-2N}$ is appropriate, where $N = 1 + \text{int}(U_I/\hbar\omega)$ is the number of photons required to overcome the ionization potential. For $\gamma \ll 1$, the tunneling formula is more accurate:

$$w(a) \cong 4\Omega_0\left(\frac{U_I}{U_H}\right)^{5/2}\frac{a_H}{a_1}\exp\left[-\frac{2}{3}\left(\frac{U_I}{U_H}\right)^{3/2}\frac{a_H}{a_1}\right],$$

with atomic frequency $\Omega_0 \cong 4.1 \times 10^{16}$ s^{-1}, hydrogen ionization potential $U_H = 13.6$ eV, and the hydrogenic electric-field normalized vector potential $a_H \cong 3.05 \times 10^{14}/\omega$. An exponential fit was used to fill in the region between the multiphoton and tunneling regimes. The molecular nature of hydrogen was approximated by using the molecular ionization potential $U_I = U_{H_2} = 15.4$ eV (Ref. 26). To conserve energy, an additional damping term on the pump was added to Eq. (1) by balancing the equation $n_c(m_e c^2/2)\partial_t a_1^2 = -(U_I + \epsilon)\partial_t n_e$, where $\epsilon = m_e v_{osc}^2/2$ is the assumed birth energy and v_{osc} is the oscillation velocity of electrons in the pump laser's electric field. The electron temperature was initialized locally at the birth energy, but it can subsequently evolve to balance collisional absorption of the pump and seed.

REFERENCES

1. D. H. Froula, D. Turnbull, T. J. Kessler, D. Haberberger, J. L. Shaw, J. Katz, and I. A. Begishev, "Flying Focus: Spatiotemporal Control of the Longitudinal Laser Beam Intensity," submitted to Nature Physics.

2. V. M. Malkin, G. Shvets, and N. J. Fisch, Phys. Rev. Lett. **82**, 4448 (1999).

3. A. A. Andreev *et al.*, Phys. Plasmas **13**, 053110 (2006).

4. L. Lancia *et al.*, Phys. Rev. Lett. **104**, 025001 (2010).

5. G. Lehmann, F. Schluck, and K. H. Spatschek, Phys. Plasmas **19**, 093120 (2012).

6. G. Lehmann and K. H. Spatschek, Phys. Plasmas **20**, 073112 (2013).

7. S. Weber *et al.* Phys. Rev. Lett. **111**, 055004 (2013).

8. L. Lancia *et al.*, Phys. Rev. Lett. **116**, 075001 (2016).

9. Y. Ping *et al.*, Phys. Rev. E **62**, R4532 (2000).

10. Y. Ping *et al.*, Phys. Rev. Lett. **92**, 175007 (2004).

11. W. Cheng *et al.*, Phys. Rev. Lett. **94**, 045003 (2005).

12. J. Ren *et al.*, Nat. Phys. **3**, 732 (2007).

13. D. S. Clark and N. J. Fisch, Phys. Plasmas **10**, 3363 (2003).

14. R. L. Berger, D. S. Clark, A. A. Solodov, E. J. Valeo, and N. J. Fisch, Phys. Plasmas **11**, 1931 (2004).

15. C. H. Pai *et al.*, Phys. Rev. Lett. **101**, 065005 (2008).

16. Y. Ping *et al.*, Phys. Plasmas **16**, 123113 (2009).

17. J. P. Farmer, B. Ersfeld, and D. A. Jaroszynski, Phys. Plasmas **17**, 113301 (2010).

18. N. A. Yampolsky and N. J. Fisch, Phys. Plasmas **18**, 056711 (2011).

19. X. Yang *et al.*, Sci. Rep. **5**, 13333 (2015).

20. J. D. Sadler, R. M. G. M. Trines, M. Tabak, D. Haberberger, D. H. Froula, A. S. Davies, S. Bucht, L. O. Silva, E. P. Alves, F. Fiúza,

L. Ceurvorst, N. Ratan, M. F. Kasim, R. Bingham, and P. A. Norreys, Phys. Rev. E **95**, 053211 (2017).

21. V. M. Malkin, G. Shvets, and N. J. Fisch, Phys. Rev. Lett. **84**, 1208 (2000).

22. Yu. A. Tsidulko, V. M. Malkin, and N. J. Fisch, Phys. Rev. Lett. **88**, 235004 (2002).

23. D. Turnbull, S. Li, A. Morozov, and S. Suckewer, Phys. Plasmas **19**, 073103 (2012).

24. D. Turnbull, S. Li, A. Morozov, and S. Suckewer, Phys. Plasmas **19**, 083109 (2012).

25. G. Vieux *et al.*, Sci. Rep. **7**, 2399 (2017).

26. D. S. Clark and N. J. Fisch, Phys. Plasmas **9**, 2772 (2002).

27. J. L. Kline *et al.*, Phys. Plasmas **13**, 055906 (2006).

28. T. P. Coffey, Phys. Fluids **14**, 1402 (1971).

29. P. Sprangle, E. Esarey, and J. Krall, Phys. Rev. E **54**, 4211 (1996).

30. L. V. Keldysh, Sov. Phys.-JETP **20**, 1307 (1965).